



The Effect of Deposition Conditions on Adhesion Strength of Ti and Ti6Al4V Cold Spray Splats

Dina Goldbaum, J. Michael Shockley, Richard R. Chromik, Ahmad Rezaeian, Stephen Yue, Jean-Gabriel Legoux, and Eric Irissou

(Submitted July 12, 2011; in revised form November 5, 2011)

Cold spray is a complex process where many parameters have to be considered in order to achieve optimized material deposition and properties. In the cold spray process, deposition velocity influences the degree of material deformation and material adhesion. While most materials can be easily deposited at relatively low deposition velocity (<700 m/s), this is not the case for high yield strength materials like Ti and its alloys. In the present study, we evaluate the effects of deposition velocity, powder size, particle position in the gas jet, gas temperature, and substrate temperature on the adhesion strength of cold sprayed Ti and Ti6Al4V splats. A micromechanical test technique was used to shear individual splats of Ti or Ti6Al4V and measure their adhesion strength. The splats were deposited onto Ti or Ti6Al4V substrates over a range of deposition conditions with either nitrogen or helium as the propelling gas. The splat adhesion testing coupled with microstructural characterization was used to define the strength, the type and the continuity of the bonded interface between splat and substrate material. The results demonstrated that optimization of spray conditions makes it possible to obtain splats with continuous bonding along the splat/substrate interface and measured adhesion strengths approaching the shear strength of bulk material. The parameters shown to improve the splat adhesion included the increase of the splat deposition velocity well above the critical deposition velocity of the tested material, increase in the temperature of both powder and the substrate material, decrease in the powder size, and optimization of the flow dynamics for the cold spray gun nozzle. Through comparisons to the literature, the adhesion strength of Ti splats measured with the splat adhesion technique correlated well with the cohesion strength of Ti coatings deposited under similar conditions and measured with tubular coating tensile (TCT) test.

Keywords adhesion, cold spray, splats, Ti, Ti6Al4V

1. Introduction

The cold spray process is based on numerous principles of gas flow, material deformation and thermodynamics (Ref 1). The coating deposition is achieved with a de-Laval type nozzle, where pressurized and preheated nitrogen or helium gas undergoes compression and expansion, imparting supersonic velocities to the feed stock powders (Ref 1). The particle velocity at which deposition takes place is known as critical velocity, which is a function of the material yield strength and temperature, and is material-dependent (Ref 2). For Ti and Ti alloys the critical velocity can be as high as 700-900 m/s

(Ref 2, 3). At the critical velocity, the leading theory for the mechanism of cold spray deposition in metals is that the high strain rate in the material leads to plastic deformation and the formation of, what is reported to be, a region of adiabatic shear instability (Ref 2, 4-7). In the adiabatic shear instability region, temperature can approach and even reach the melting point of material thus leading to viscoelastic material flow, formation of a conformal interface, and metallurgical bonding (Ref 4, 5, 8).

The cold sprayed particles that undergo deformation and adhere to the substrate material are often referred to as splats. The deposition mechanisms of splats vary depending of the in-flight particle velocity, henceforth “deposition velocity”, and typically follow three generally accepted deposition mechanisms (Ref 1-3, 5, 6, 9-13). At the deposition velocity below but approaching the critical velocity, the material undergoes plastic deformation that is measured as a function of splat width divided by the splat height and referred to as splat flattening ratio or FR (Ref 10, 14). At velocity below the critical velocity, the transition to the adiabatic shear instability is limited and results in limited metallurgical bonding (Ref 2, 3, 5). For that reason, the bonding between the splat and the substrate is mostly through a weak conformal adhesion from mechanical interlocking of asperities. Figure 1(a) illustrates this deposition mode.

Dina Goldbaum, J. Michael Shockley, Richard R. Chromik, Ahmad Rezaeian, and Stephen Yue, Department of Mining and Materials Engineering, McGill University, 3610 University Street, Montreal, QC H3A 2B2, Canada; and Jean-Gabriel Legoux and Eric Irissou, Industrial Materials Institute, National Research Council Canada, Boucherville, QC, Canada. Contact e-mail: Richard.chromik@mcgill.ca.

As the deposition velocity surpasses the critical velocity, Fig. 1(b), the formation of the adiabatic shear instability becomes more pronounced leading to a viscoelastic material flow. During splat deformation, the material flows in an outward direction from the impact region, resulting in material jetting. The jetting contributes to an increase in the length of the interface between the splat and the substrate and increase in the splat flattening ratio. The formation of adiabatic shear instability and increase in the length of the splat-substrate interface leads to a greater fraction of metallurgical bonding and a stronger splat adhesion (Ref 5, 11).

Another type of the deposition behavior is often observed for splats deposited at velocities significantly higher than the critical velocity. The deformation takes place not only in the cold sprayed materials but also in the substrate material. The intimate contact between the splat and the substrate contributes to a more continuous, void or oxide free, bond between two interfaces and even stronger splat adhesion as can be seen in Fig. 1(c) (Ref 9, 13).

Figure 1 illustrates three commonly known deposition mechanisms in cold spray splats. However, not all the splats in the jet undergo deposition. When the particle velocity is lower than the critical velocity, some particles do not deposit and instead rebound from the substrate

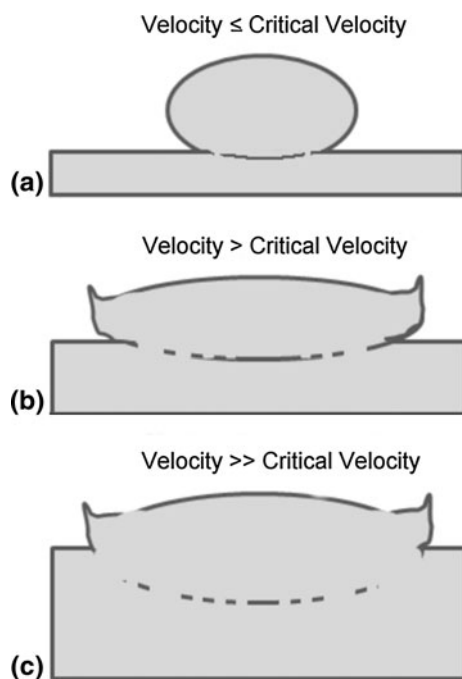


Fig. 1 General appearance of cold sprayed splats as a function of particle velocity with respect to the critical velocity. When the particle velocity is low (a), deformation takes place, but very little adiabatic shear. At medium particle velocities (b), there is significant deformation of the splat and formation of adiabatic shear and metallurgical bonding in these local regions. However, the substrate remains undeformed. At the highest particle velocities (c), both the splat and substrate deform extensively and a combined adiabatic shear process leads to an increase in the length of the conformal interface and an increase in the density of regions that have become metallurgically bonded

(Ref 1, 3, 15). The rebound phenomenon is attributed to the elastic strain energy stored in the material which counteracts the impact forces. Similarly, at very high deposition velocity, the elastic strain energy can surpass the bonding energy and can lead to splat erosion (Ref 16, 17). The elastic strain energy is typically highest at the center of the impact and contributes to the particle debonding and void formation in that region (Ref 16, 17). Void formation may occur in the rebound region, as indicated by the dotted lines at the center of the splat in Fig. 1(b) and (c).

A number of particle impact simulations have been used to understand the deposition mechanisms of metals like copper and aluminum onto copper or aluminum substrates, as well as titanium and its alloys onto steel and titanium substrates (Ref 2, 3, 5, 8, 9, 13, 18, 19). The deposition velocity was shown to have a significant effect on the particle deformation (Ref 10) and adhesion (Ref 9, 11) but was also predicted to affect the temperature rise in the adiabatic shear instability region (Ref 3, 5, 9). Recent studies indicate that other parameters such as particle impact temperature (Ref 17) and substrate temperature (Ref 20) may also affect the cold spray deposition process (Ref 1, 11). Higher impact temperature of the splats or substrate lowers the critical velocity required for the cold spray deposition (Ref 3) and was shown to contribute to a better splat adhesion to a substrate material as well as to the particle cohesion strength in the coating (Ref 11, 21). Particle and substrate temperature were also shown to vary with gas preheat temperature (Ref 2, 21, 22). Other parameters expected to affect the cold spray deposition process include the powder size (Ref 3, 23), particle position in the gas jet (Ref 24) and particle impact angle (Ref 21).

Because the bonding process for cold spray takes place at the “splat level,” a measurement of the adhesion of a single splat to a substrate provides a fundamental measurement of the bonding, and can, in some circumstances, be a good indicator of the cohesive strength in a coating (Ref 25). To date, there are only a few reports in the literature of methods for measuring the adhesion of the cold sprayed splats. We have developed a micromechanical test technique that measures the splat adhesion strength (Ref 11), where, in the previous report, the technique was termed a “modified ball bond shear test” due to its similarity to ball bond shear testing of solder bumps (Ref 26). Since our original report, Dickinson and Yamada (Ref 27) developed a method similar to ours for testing of TiO₂ ceramic cold sprayed particles on stainless steel substrates. Other groups have developed a method using a laser shock adhesion test (LASAT) that measures the bonding strength for splats present over a roughly 1 cm² area (Ref 9).

The present study expands significantly on a previous report using the splat adhesion test on Ti splats on Ti substrates (Ref 11), which focused primarily on the effect of spray conditions for Ti splats sprayed with nitrogen gas. In the present study, the effect of spray conditions on splat adhesion strength are explored again, but now for both Ti and Ti6Al4V splats sprayed with both helium and nitrogen gasses onto substrates held at room temperature or

pre-heated to 400 °C. Also, testing was performed on varied splat sizes and on splats at varied position across a single deposition pass in order to test the effect of the particle size and the particle position in the gas jet on the splat adhesion strength. Light optical microscopy (LOM) and scanning electron microscopy (SEM) were used for the evaluation of the splat deformation mechanisms and characterization of the splat substrate bonding interface. Three splat shearing regimes were identified by observation of residual shear tracks on the substrate surface and the features in the force-displacement curves, which were recorded during the shearing of the splats. The present study explores a wide range of deposition conditions for Ti and Ti6Al4V and uses the splat adhesion test and other characterization methods to determine those conditions leading to high adhesion strength. Results for adhesion at the splat level are compared to bond strength and cohesion strength measurements for Ti reported in the literature.

2. Experimental Procedure

2.1 Cold Spray Deposition

Cold spray splats were obtained by powder acceleration with a Kinetiks 4000 cold spray gun (CGT GmbH, Germany) through a MOC24 nozzle for deposition using nitrogen as propellant and through a VH70 nozzle (ASB Industries Inc., Barberton, USA) for deposition using helium as propellant. A powder feeding rate of 1-2 g/min and a gun traverse speed of 1 m/s were used. Powders of commercially pure (CP) Ti or Ti6Al4V powders (Raymore Inc., Boisbriand, QC, Canada) were cold sprayed onto substrates of the same material, where the substrate was either heated or left at ambient conditions. The powder size distribution for both powders was measured to be between 0 and 80 μm with 29 μm averaged particle diameter as was published previously (Ref 28). SEM micrographs of the powders are given in Fig. 2. The substrates were annealed Ti or Ti6Al4V plates with 3 mm plate thickness and a milled finish (McMaster-Carr, Aurora, OH, USA). The substrates were degreased with

acetone prior to the cold spray splat deposition but were otherwise left in the as-received surface state. For some depositions, the Ti or Ti6Al4V substrates were preheated to 400 °C with a custom-built sample holder with three heating elements. A thermocouple was placed inside the sample holder and a temperature of 400 °C was maintained through the cold spray deposition of splats.

The particle velocity was measured, in a free jet, with a DPV2000 (Tecnar Automation, St. Bruno, QC, Canada). Velocities ranging from 580 to 1140 m/s were obtained by preheating and pressurizing nitrogen or helium gas from 25 to 800 °C and from 1 to 4 MPa. The velocity of 1000-2000 particles was measured and averaged for each deposition condition. For the deposition conditions with nitrogen gas, the velocity measurements were carried out at 4 cm distance from the gun nozzle. For the deposition conditions with helium gas, the distance from the nozzle was maintained at 8 cm. The same gun nozzle-substrate distance was used during cold spray deposition of splats.

2.2 Microstructural Characterization

The cold sprayed samples were cut in cross-section and mounted into the cold mount epoxy. The samples were then polished according to a standard polishing procedure for Ti (Ref 29) with a final step of 0.05 μm colloidal silica with 10% hydrogen peroxide. The samples were then etched with Kroll's reagent consisting of 3% HNO_3 , 2% HF and distilled water to reveal the splat/substrate bonded interface.

The etched images of splats were examined with light optical microscope (LOM) and a variable pressure scanning electron microscope (Hitachi S-3000N VP-SEM, Japan). Image analysis software (Clemex Vision Professional 5.0, Clemex Technology Inc., Longueuil, QC, Canada) was used to measure the height and width of the cold spray splats from LOM images of splat cross-sections. The splat width, w , and height, h , were then used to calculate the splat flattening ratio. Flattening ratio is a measure of the degree of splat deformation and is described in Eq 1 (Ref 8, 10, 30). Typically, a flattening ratio of 10-30 splats was calculated and an average value was taken for each deposition condition. In the case of low deposition velocities (below 650 m/s), the deposition

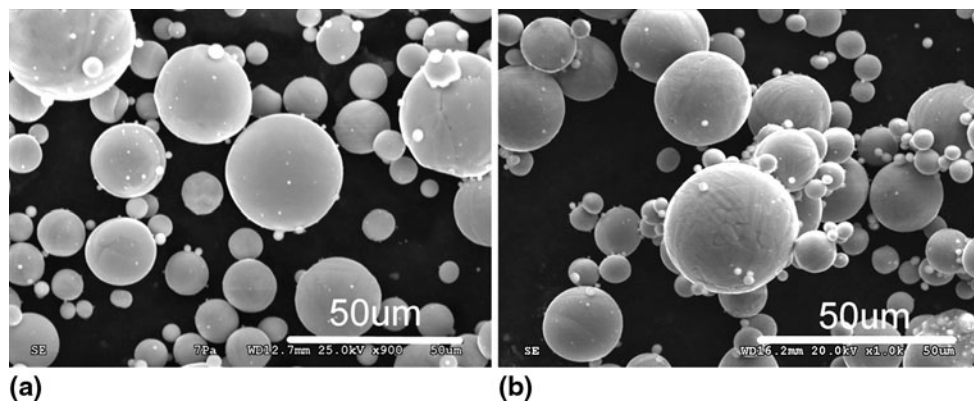


Fig. 2 Micrographs obtained by SEM for the (a) Ti powder and (b) Ti6Al4V powder

efficiency of splats was very low and for that reason the average of 3 or more splats was taken. The standard deviation on the mean was used as the error bar.

$$FR = \frac{w \text{ (}\mu\text{m)}}{h \text{ (}\mu\text{m)}} \quad (\text{Eq 1})$$

The flattening ratio was only measured for splats that were polished near the center of the splat. The definition of the splat center was made possible by the transparent nature of the cold mount epoxy and the topographical SEM imaging. We estimate that our measurements are made within $\pm 2 \mu\text{m}$ from the splat center. Splat-cross sections in the vicinity of the splat center were found to be self-similar and thus the flattening ratio measurements were not significantly affected by small offsets of the splat cross-section from the actual position of the splat center.

2.3 Mechanical Property and Surface Characterization of Starting Materials

The hardness of the Ti and Ti6Al4V feed-stock powder and Ti and Ti6Al4V substrates was measured by nanoindentation with two systems, either Ubi 3 or Triboindenter (Hysitron Incorporated, Minneapolis, MN). The hardness and reduced elastic modulus were measured with a Berkovich tip at 1 mN load, 200 $\mu\text{N/s}$ loading/unloading rate and 1 s holding time. Data was analyzed using the Oliver and Pharr method (Ref 31). Average property values were taken from over 40 data points.

The surface roughness of the substrates was measured with a contact profilometer (Veeco Instruments, CA, USA). The average surface roughness (R_a) was determined from 6 line scans of 1 cm in length carried at 1.25 mm/s and 10 mg load on Ti and Ti6Al4V substrate. The scans were carried along and across the substrate length.

2.4 Splat Adhesion Testing

Shear testing was performed with a Micro-Combi Scratch Tester (CSM Instruments, Inc., Needham, MA, USA) equipped with a wedge shaped stylus (Ref 11). The adhesion strength of the splats was measured by applying a normal force, F_N , of 30 or 300 mN onto the stylus (100 μm in width) that was placed on a substrate a distance of approximately 30-40 μm away from the splat. The substrate was then moved at 150 $\mu\text{m/min}$ rate below the stylus, as indicated schematically in Fig. 3.

The adhesion strength of the splat was calculated as a function of tangential force, F_T , exerted on the stylus, the baseline force F_B and the splat area, A , according to Eq 2. The splat area was measured prior to splat shearing according to Eq 3, where w is splat diameter measured with the LOM on the scratch tester by taking the average width of the splat in two orthogonal directions. Splats were imaged in plan view.

$$\text{Adhesion strength (MPa)} = \frac{F_T - F_B}{A} \quad (\text{Eq 2})$$

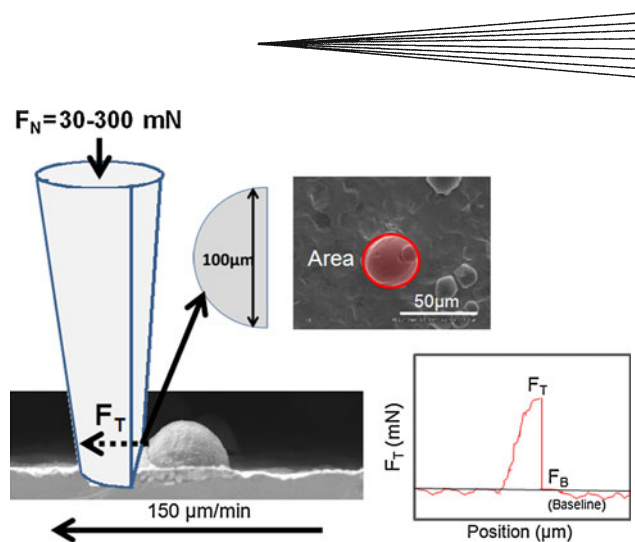


Fig. 3 A schematic diagrams of splat adhesion testing. On the left, a cross-sectional view and, on the upper-right, a top-down view of the test are provided. In the upper right, the cross-section area of the splat is noted, which is used in the calculation of the splat adhesion strength. In the lower-right, an example of the force-displacement curve obtained during the shearing of a splat

$$A = \pi \left(\frac{w}{2} \right)^2 \quad (\text{Eq 3})$$

For each deposition condition, 5-10 splats were tested. A narrow range of splat diameters, as observed with the microscope on the scratch tester, were chosen for each sample such that a similar pre-impact diameter was tested for all conditions. The particle pre-impact diameter was calculated by assuming that upon the impact the splats deform from a spherical geometry into oblate spheroid geometry and according to Eq 4:

$$d \text{ (}\mu\text{m)} = (w^2 h)^{1/3} = \left(\frac{w^3}{FR} \right)^{1/3} \quad (\text{Eq 4})$$

where the splat width, w , was measured as described above for Eq 3 and FR was determined according to Eq 1 from splat cross-sections for each deposition condition. The average pre-impact diameter of the tested splats for all deposition conditions was calculated to be $34 \pm 5 \mu\text{m}$, and was close to the average size of the particles in the feed-stock powder (29 μm). The assumption of the oblate spheroid geometry has been used in the past in a method developed by Kim et al. (Ref 17) which uses an image analysis routine to measure the entire area of a splat cross-section. Our method, using Eq 4, is a simpler version that can be used to estimate the pre-impact diameters for splats that are tested by the splat adhesion technique. A comparison between results from the two methods applied to splat cross-sections found that the pre-impact diameters agree within experimental error.

3. Results

3.1 Mechanical Property Characterization

In Table 1 the hardness and reduced elastic modulus of the feedstock Ti and Ti6Al4V powder as well as Ti and

Ti6Al4V substrates are summarized. The average hardness of the commercially pure Ti powder and Ti substrates were the same at 3.1 GPa with reduced modulus of each material very close to the Young's modulus of Ti. The hardness of the Ti6Al4V powder and substrate was higher than that of the pure Ti at 4.8 and 5.8 GPa respectively.

In Table 1, the average surface roughness of as received Ti and Ti6Al4V substrates is also listed. Both substrates demonstrate comparable R_a values that fall within the standard deviation on each measurement.

3.2 The Effect of the Gas Temperature and Pressure on the Deposition Velocity

Ti or Ti6Al4V powder was deposited onto Ti or Ti6Al4V substrate at velocities ranging from 580 to 1140 m/s, which were obtained by varying the nitrogen or helium gas temperature from 25 to 800 °C and by changing the gas inlet pressure from 1 to 4 MPa. The average deposition velocity increased with increase in the gas temperature but also increased with increase in the inlet

gas pressure. At similar gas preheat temperature and pressure, higher velocities were obtained with helium gas when compared to nitrogen gas. The deposition conditions and the corresponding average deposition velocities are listed in Table 2.

In Table 2, some of the samples (as indicated) were produced at different time frame, within a period of 1 year from when most of the splats were produced, and the deposition velocity for a given gas preheat temperature and pressure condition was re-measured prior to sample preparation. The difference in the particle velocities can be attributed to the changes made in the cold spray system over time including the replacement of the gun nozzle. Some of the particle velocity measurements, listed in the Table 1, were previously published (Ref 11, 25).

While the gas temperature and pressure are the main parameters affecting particle velocity, other parameters such as the particle position in the gas jet (Ref 24) and the size of the powder particles (Ref 3) can also have an effect on the particle velocity. The particles located at the edge of the jet travel at a lower speed when compared to particles propelled at the center of the jet (Ref 24). At the same time, smaller particles travel at a faster speed than larger particles (Ref 3). Due to these facts, the actual velocity for each deposition condition follows a Gaussian distribution as shown in Fig. 4.

In Fig. 4, three particle velocity distributions for low, intermediate and high deposition velocity conditions are shown. At low deposition conditions, although the average velocity is 625 m/s, a small portion of particles reach the minimum critical velocity for Ti ranging between 700 and 900 m/s (Ref 3). Similarly, at high deposition condition

Table 1 Properties of Ti and Ti6Al4V powder and substrates

Material	Hardness, GPa	Reduced elastic modulus, GPa	Surface roughness R_a , μm
Ti powder	3.1 ± 0.4	114 ± 10	...
Ti substrate	3.1 ± 0.3	125 ± 6	0.60 ± 0.12
Ti6Al4V powder	4.8 ± 0.3	104 ± 5	...
Ti6Al4V substrate	5.8 ± 1.1	123 ± 11	0.52 ± 0.14

Table 2 Splat deposition conditions

Gas	Ti powder on Ti (at RT and at 400 °C)			Ti6Al4V powder on Ti6Al4V (at RT and at 400 °C)		
	Gas temperature, °C	Gas pressure, MPa	Deposition velocity, m/s	Gas temperature, °C	Gas pressure, MPa	Deposition velocity, m/s
Nitrogen	300	2	580	300	2	590
	300	3	625	300	3	631
	300	4	642	300	4	657
	500	2	636	500	2	646
	500	3	694	500	3	701
	500	4	724	500	4	741
	750	3	770	750	3	778
	800	4	825-852(a)	800	4	834
Gas	Ti on Ti (at RT)			Ti6Al4V on Ti6Al4V (at RT)		
	Gas temperature, °C	Gas pressure, MPa	Deposition velocity, m/s	Gas temperature, °C	Gas pressure, MPa	Deposition velocity, m/s
Helium	50	1	616	25	1	562
	50	2	787	25	2	787
	50	3	877
	350	2	877	350	2	964
	350	3	950	350	3	1052
	350	4	1140	350	4	1115

(a) Particle velocity measured at a different time frame

where most of the particles travel at an average deposition velocity of 770 m/s some of the particles travel below the minimum critical velocity.

To circumvent some of the uncertainty in the particle velocity measurements, mainly the splats at the center of the deposition pass were examined. This position corresponds to particles near the center of the gas jet, where the velocity is the highest. Furthermore, measurements were carried out on particles close to the average feed-stock powder diameter of 29 μm , removing some of the variation in velocity associated with particle size. Additionally,

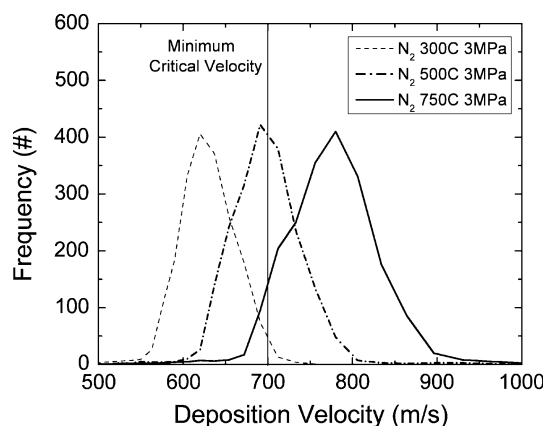


Fig. 4 Particle velocity distribution for low, intermediate and high deposition conditions of Ti powder accelerated with nitrogen gas. The minimum critical velocity for Ti is indicated by vertical intercept at 700 m/s and according to Schmidt et al. (Ref 3)

these particles are the most populous within the velocity distributions, such as those in Fig. 4. Thus, it is expected that particles tested in this manner arrived at the average velocity for the given spray condition. Other testing was carried out as a function of splat position across the deposition pass or as a function of splat size along the center of the deposition pass. In these cases, the variation in properties measured is a function of velocity, due to its variation across the gas jet and with splat size.

3.3 Effect of Particle Velocity and Preheat Temperature on Splat Deposition

In Fig. 5, representative SEM images of the etched Ti (a-c) and Ti6Al4V (d-f) splats deposited at increasing deposition velocities are shown. Ti splats deposited on Ti substrate as well as Ti6Al4V splats deposited on Ti6Al4V substrate showed three different deposition regimes. As can be seen in Fig. 5(a) and (d), at deposition velocity approaching the critical velocity (~ 700 m/s), the splat deformation was not extensive and material jetting region was limited. Bonding took place mainly through conformal adhesion between the splat and the substrate. As the deposition velocity increased, the splats became more deformed and extensive material jetting took place, as can be seen in Fig. 5(b) and (e). Regions of continuous bonding was observed in the splat at 45° angle from the splat impact site while a void formation was observed at the center of the splat/substrate interface.

As the deposition velocity increased even further, substrate deformation became more pronounced (see

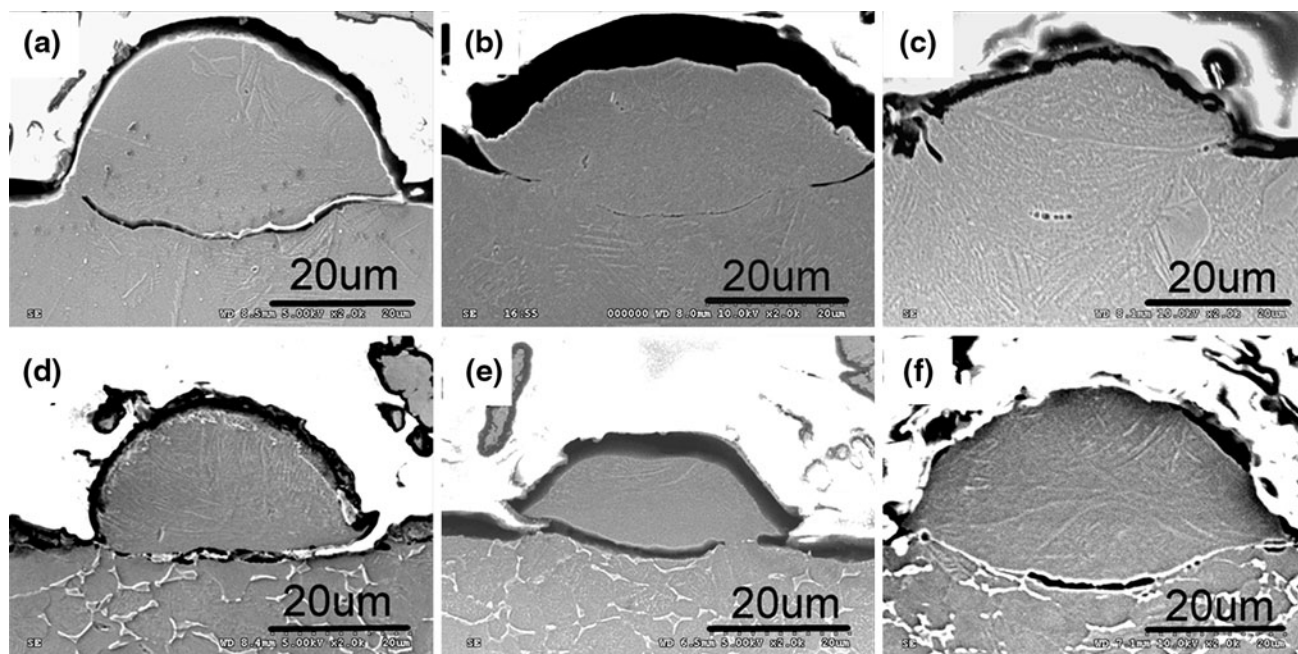


Fig. 5 Etched SEM cross-sectional micrographs of Ti splats deposited on Ti at (a) 724 m/s (N₂ at 500 °C 4 MPa), (b) 825 m/s (N₂ at 800 °C 4 MPa), (c) 1140 m/s (He at 350 °C 4 MPa) and Ti6Al4V splats deposited on Ti6Al4V substrate at (d) 741 m/s (N₂ at 500 °C 4 MPa), (e) 834 m/s (N₂ at 800 °C 4 MPa), (f) 1115 m/s (He at 350 °C 4 MPa). The dark regions between the splat and the substrate indicate regions of poor bonding and void formation

Fig. 5c). The substrate deformation contributed to the formation of an intimate, possibly metallurgical, contact between the Ti splat and substrate. Under the same deposition conditions, Ti6Al4V splats deposited on Ti6Al4V showed a lower degree of substrate deformation and bonding when compared to Ti splats deposited on Ti (see Fig. 5e). The bonding interface between the Ti6Al4V splat and substrate was not continuous, as can be seen in Fig. 5(f).

The splat deformation was measured in terms of flattening ratio, from the etched images of splats similar to the ones shown in Fig. 5 and according to Eq 1. The flattening ratio was plotted as a function of particle deposition velocity (see Fig. 6). As can be seen in Fig. 6(a), the Ti splat flattening ratio increased with increase in the deposition velocity up to 850 m/s but then stabilized and slightly decreased at 1140 m/s. Similar splat deformation behavior was observed in etched splat cross-sections shown in Fig. 5(a)-(c). The splat deposited at 825 m/s was more deformed than the splat deposited at 724 m/s however the splat deposited at 1140 m/s had a lower flattening ratio. At 1140 m/s a significant increase in the substrate deformation was observed. Average Ti substrate deformation depth was calculated from SEM images of 10-30 etched splat cross-sections and was measured to be

$2.1 \pm 2.2 \mu\text{m}$ at 825 m/s and $8.1 \pm 4.3 \mu\text{m}$ at 1140 m/s which is approximately 10 and 40% of the splat height.

The flattening ratio of Ti6Al4V splats, shown in Fig. 6(b), increased from roughly 2.0 at 650 m/s to 3.0 at deposition velocity of 850 m/s. The splat flattening ratio did not increase at higher deposition velocities obtained with helium gas. The cross-sectional SEM image of the splat deposited at 1115 m/s (see Fig. 5f) had very limited substrate deformation compared to the Ti substrate seen in Fig. 5(c). Deformation depth for Ti6Al4V substrates increased from $0.5 \pm 1.3 \mu\text{m}$ at 834 m/s (which is similar to the roughness of the substrate) to $4.6 \pm 1.6 \mu\text{m}$ at 1115 m/s.

A steady increase in the splat adhesion strength was observed with increase in the splat deposition velocity, as seen in Fig. 7. For Ti splats deposited on Ti substrates at velocities greater than 800 m/s, the splat adhesion strength approached the shear strength of Ti at 380 MPa (Ref 32). The results correlated well with the SEM image shown in Fig. 5 that showed an increase in the splat/substrate bonded interface with increase in the splat deposition velocity.

The adhesion strength of Ti6Al4V splats deposited on Ti6Al4V substrate was lower than that of Ti splats deposited on Ti substrate and was significantly lower than the shear strength of Ti6Al4V at 550 MPa (Ref 32). The

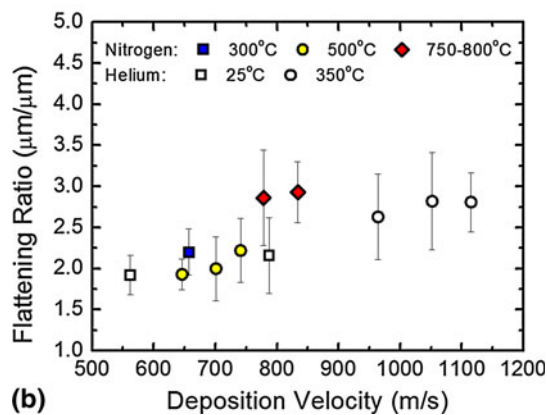
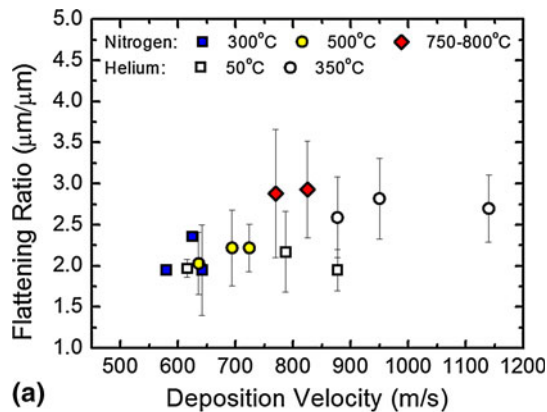


Fig. 6 Flattening ratio vs. deposition velocity for (a) Ti splats and (b) Ti6Al4V splats deposited with nitrogen and helium gases at varied gas preheat temperatures. No Ti6Al4V splats, deposited with nitrogen gas, were found below 650 m/s

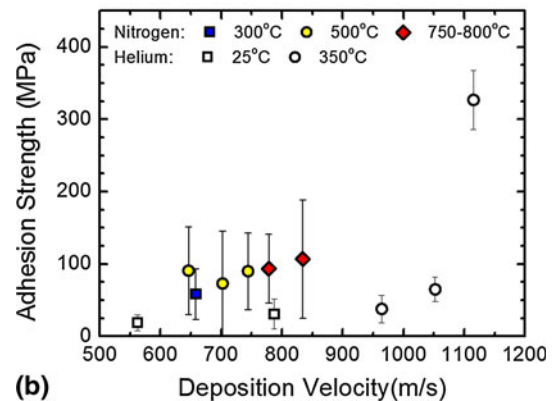
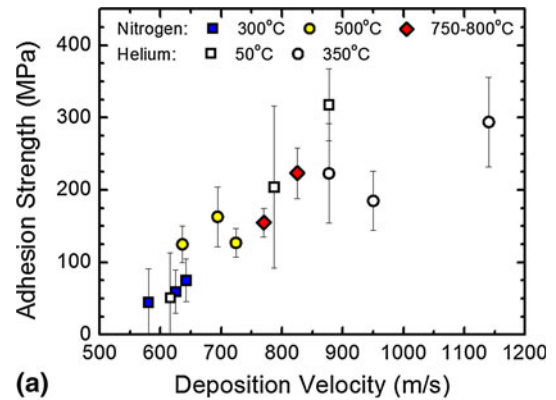


Fig. 7 Adhesion strength vs. deposition velocity for (a) Ti splats deposited on Ti substrate and (b) Ti6Al4V splats deposited on Ti6Al4V substrate with nitrogen and helium gases at varied gas preheat temperatures. No Ti6Al4V splats, deposited with nitrogen gas, were found below 650 m/s

adhesion strength for the Ti6Al4V splats was mostly constant at 100 MPa but reached ~ 320 MPa at a the highest deposition velocity of 1115 m/s. Ti6Al4V has higher shear strength when compared to pure Ti and higher impact velocities are required to induce adiabatic shear.

3.4 Splat Shearing Behaviors

During the adhesion testing, three types of splat shearing regimes were observed and are shown in Fig. 8. In the first shearing regime, a rapid increase in the tangential forces with respect to the stylus displacement was observed and was followed by a rapid drop in the tangential forces. The total stylus displacement associated with the shearing event was smaller than the width of the splat. Also, the very small rise in the tangential forces (~ 15 mN) with tip displacement indicates poor splat adhesion strength (12 MPa). The sheared region showed a presence of the crater in place of the sheared splat with no visible shear tracks (see Fig. 8 regime 1b) indicating that the splat adhesion occurred was mainly through a weak conformal bonding. First shearing regime was typically observed for splats deposited below the critical velocity (700 m/s for Ti).

In second shearing regime, the rise in the tangential forces occurred over a wider displacement range than in regime 1. In Fig. 8, the peak tangential force reached 300 mN and was followed by a rapid drop in the tangential force half way into the splat. Splats demonstrating regime 2 shearing behavior also had higher adhesion strength (239 MPa) compared to those in regime 1. Regime 2 shearing behavior was observed in Ti splats deposited on Ti substrate at 825 m/s and in Ti6Al4V splats deposited on Ti6Al4V substrate at 1115 m/s. Examination of the sheared region on the substrate revealed shear tracks that formed a ring around the impact crater. The ring formation had the outline of the sheared splat that correlated with the region of continuously bonded interface observed from the splats cross-sections in Fig. 5(b) and (f).

Finally, the third shearing regime was defined by a smooth rise and drop in the tangential forces during the shearing of the splat. As compared to regimes 1 or 2, regime 3 had no drastic drop in the tangential forces at the end of the shearing event and the width of the tangential force peak was roughly the width of the sheared splat. For the third shearing regime, the shear tracks formed a full circle with no crater formation. The splats demonstrating this type of shearing behavior had adhesion strength approaching the theoretical shear strength. The third

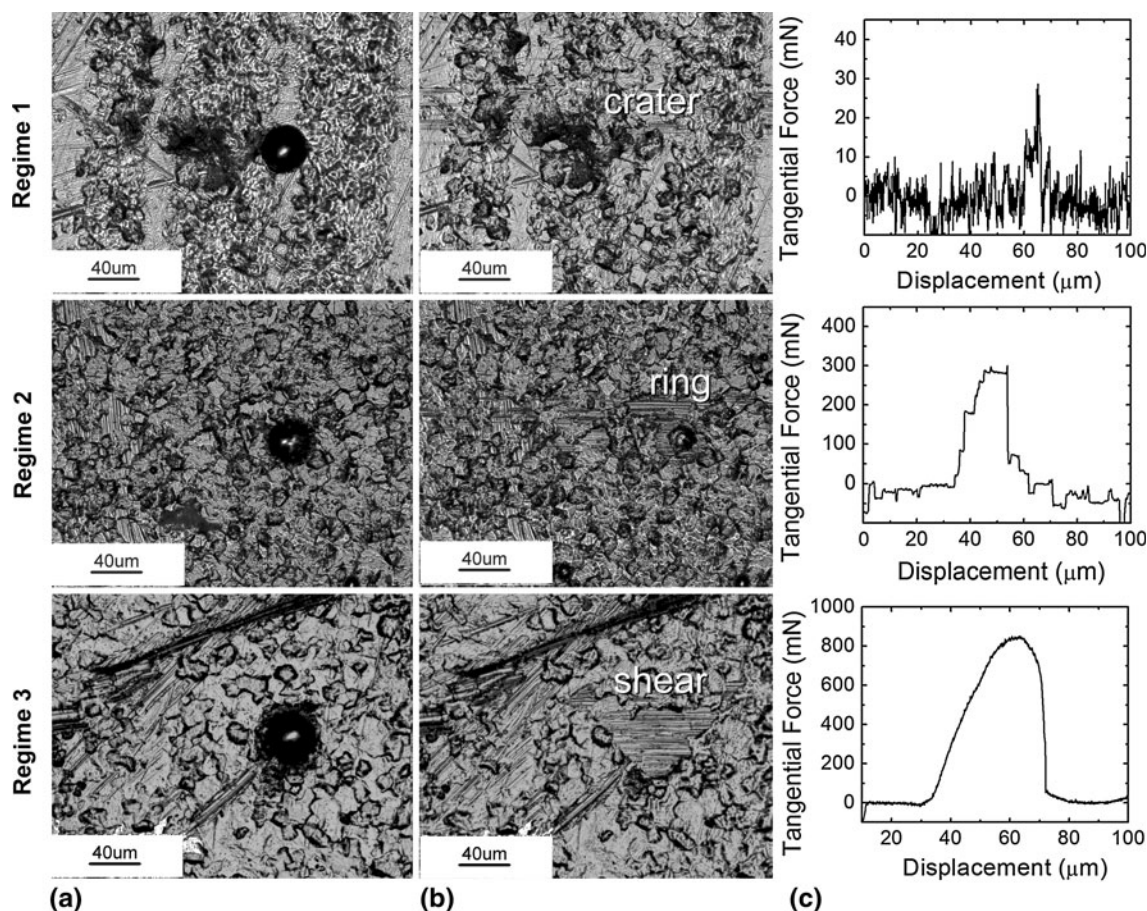


Fig. 8 Three regimes of splat shearing behavior are shown with corresponding top view LOM images of splats (a) before shearing and (b) after shearing, and (c) with respective tangential force vs. displacement curves

shearing regime was observed for Ti splats deposited at 1140 m/s. The average adhesion strength of the splats deposited at this velocity was measured to be 294 MPa, below the shear strength of Ti. The cross-sectional image of a splat deposited at this velocity is shown in Fig. 5(c), where it is seen that not all of jetting region participated in the splat bonding. Thus, the actual splat contact area calculated according to Eq 3 was slightly overestimated and may explain why splats shearing according to regime 3 do not have adhesion strength closer to the actual shear strength of Ti. Ti6Al4V splats deposited on Ti6Al4V substrate did not demonstrate regime 3 shearing behavior and sheared according to regime 2 at 1115 m/s.

In Fig. 9, SEM images of a sheared region on a Ti substrate are shown for a condition that exhibited regime 2 behavior. Three features of splat shearing behavior are observed and include the crater formation which is surrounded by a ring of the shear tracks and finally the shear tracks themselves. The shear tracks (shown in Fig. 9a) formed a ring in the shape of the sheared splat. The inside of wall of the shear track ring contained fine dimples (see in Fig. 9b) that were produced as the splat was de-bonded from the substrate. The dimples are indicative of a ductile fracture in Ti and Ti6Al4V (Ref 33-36) and point to a metallurgical bonding in that region. At the center of the ring, a crater formation was observed. The center of the crater had a smooth, dimple-free surface which shows that no metallurgical bonding took place in that region. Regime 2 shearing behavior was typically observed for splats deposited above 800 m/s. The observations of where bonding took place in the sheared region correlated well with the regions of continuously bonded interface seen from SEM images of the splat deposited at 825 m/s and shown in Fig. 5(b).

3.5 Effect of Powder Particle Size and Position in the Gas Jet

In the previous sections, the adhesion strength was measured for splats with similar pre-impact particle diameter of $\sim 34 \mu\text{m}$ calculated according to Eq 4. In industrial applications, powder size distribution will vary

and a better understanding of the effect of the particle size on the adhesion strength of splats is required. In Fig. 10, the effect of the particle size on the splat adhesion strength was evaluated. As can be seen in Fig. 10, the adhesion strength of smaller splats was higher when compared to larger splats. The splats, with an estimated particle pre-impact diameter between 10 and 20 μm , had adhesion strength in the range of 250-300 MPa, while 40-60 μm splats have particle adhesion strength ranging between 150 and 250 MPa. The results correlated well with the general understanding of the particle flight dynamics where particles of smaller size were shown to have a higher in-flight velocity when compared to particles of larger size (Ref 2, 37) and consequently had a better adhesion strength.

The powder particle position in the gas jet can have an effect on the particle velocity. A particle in the center of the gas jet travels at a higher velocity than the splats at the edges of the jet (Ref 24). The particle deformation and bonding strength can be therefore affected. In Fig. 11, the

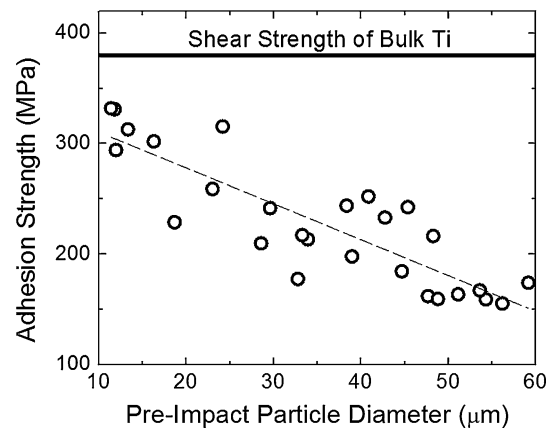


Fig. 10 The adhesion strength of Ti splats deposited at 852 m/s (N_2 800 $^\circ\text{C}$ and 4 MPa) with respect to the particle size calculated according to Eq 4. Splat adhesion was measured at the center of the deposition track. A decrease in the particle adhesion strength was observed with increase in the particle size

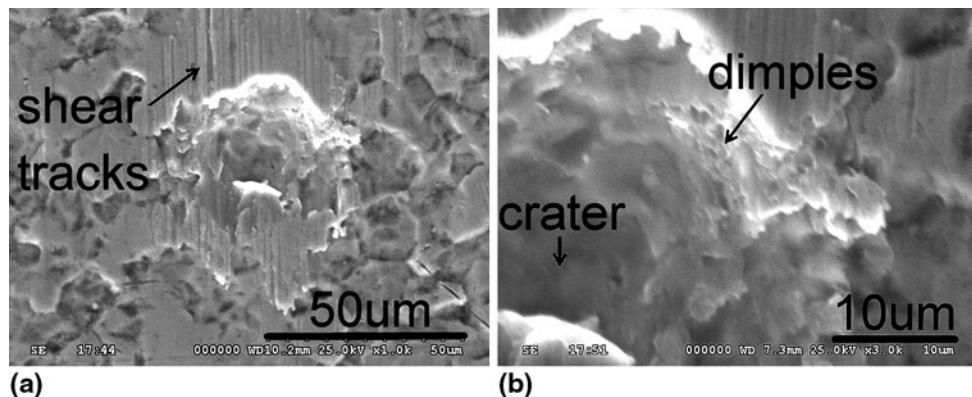


Fig. 9 SEM image of the regime 2 sheared region at low (a) and at high (b) magnification. The shear band rings surrounding the crater are shown with dimpled ductile fracture at the inside rim of the crater

splat adhesion strength was measured across the width of a deposition pass (i.e. perpendicular to the gun traverse direction). The adhesion strength of splats with roughly same particle diameter ($\sim 34 \mu\text{m}$) was measured. The splat adhesion strength was highest ($\sim 250 \text{ MPa}$) in the 4-8 mm which corresponded to the center of the pass width. Lower

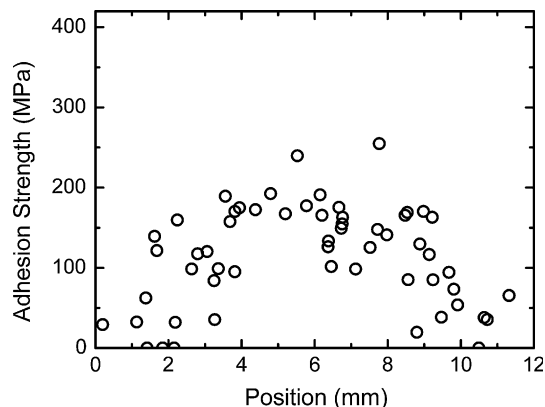


Fig. 11 Adhesion strength of Ti splats as function of their position across the deposition pass. These splats were deposited at $800 \text{ }^\circ\text{C}$ 4 MPa gas conditions and splats tested had a $\sim 29 \mu\text{m}$ particle pre-impact diameter. Lower adhesion strength is measured for splats deposited at the edge of the pass

adhesion strength, ranging from 0 to 100 MPa, was measured for the splats located at the edge of the pass at 0-4 and 8-12 mm.

3.6 Substrate Temperature Effect

The splats presented in the previous sections were deposited as a single pass at high gas traverse speed and on the substrate at room temperature. Previous studies have shown that the temperature of the substrate material increases due to heat transfer from the impingement of the pre-heated gas jet (Ref 20, 38). As a result of splat impact with the substrate and adiabatic shear, the temperature of the substrate will rise as well (Ref 1, 6, 22, 38). In order to “simulate” the substrate temperature rise due to the gas jet and successive impacts, substrates were preheated to $400 \text{ }^\circ\text{C}$ prior to splat deposition. Measurements of the adhesion strength from these splats may mimic more closely the bonding that takes place in a full coating.

As can be seen in Fig. 12(a) and (b), Ti splats deposited on preheated Ti substrate showed a more extensive bonded interface when compared to Ti splats deposited on Ti substrate at ambient temperature under same deposition conditions, as shown in Fig. 5(a) and (b). Furthermore, Ti splats deposited at 825 m/s (see Fig. 12b) showed similar substrate deformation and bonding as one obtained at much higher deposition velocity with ambient substrate

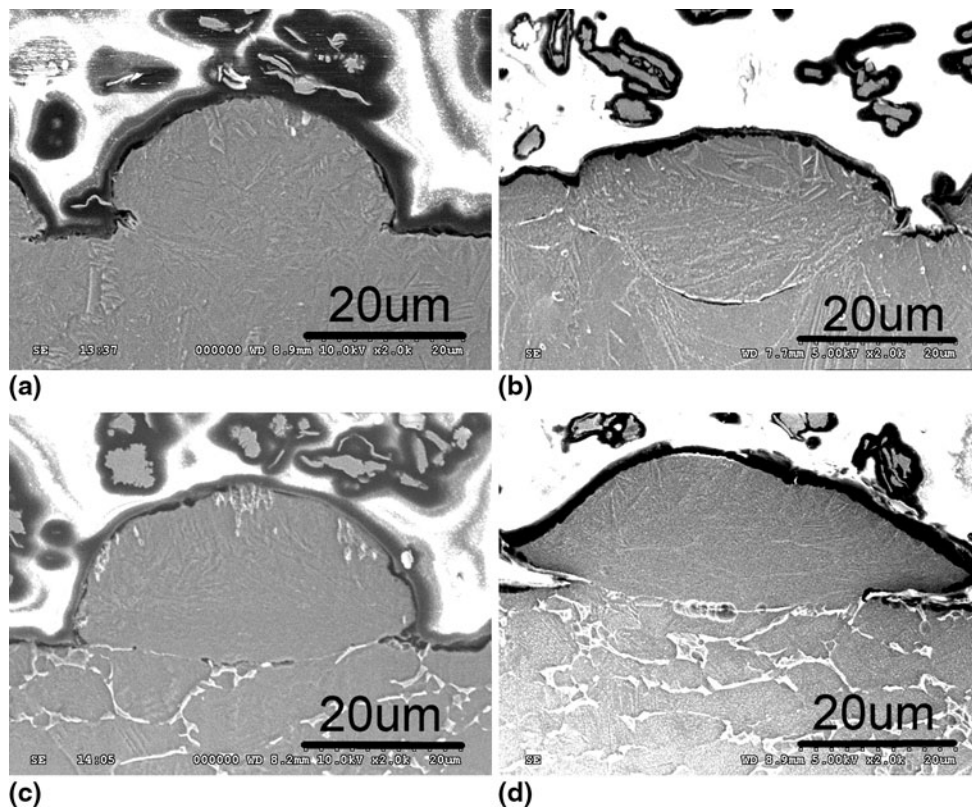


Fig. 12 Etched cross-sectional micrographs obtained with SEM for (a) Ti splats deposited at 724 m/s (N_2 at $500 \text{ }^\circ\text{C}$ 4 MPa) on Ti substrate preheated to $400 \text{ }^\circ\text{C}$, (b) Ti splats deposited at 825 m/s (N_2 at $800 \text{ }^\circ\text{C}$ 4 MPa) on Ti substrate preheated to $400 \text{ }^\circ\text{C}$, (c) Ti6Al4V splat deposited at 741 m/s (N_2 at $500 \text{ }^\circ\text{C}$ 4 MPa) on Ti6Al4V substrate preheated to $400 \text{ }^\circ\text{C}$, and (d) Ti6Al4V substrate deposited at 832 m/s (N_2 at $800 \text{ }^\circ\text{C}$ 4 MPa) on Ti6Al4V substrate preheated to $400 \text{ }^\circ\text{C}$

conditions (see Fig. 5c). The average depth of the preheated Ti substrate deformation was measured to be $4.2 \pm 2.8 \mu\text{m}$ and was higher than for the non-preheated substrate at $2.1 \pm 2.2 \mu\text{m}$ measured for 825 m/s deposition condition. Ti6Al4V splats deposited on preheated Ti6Al4V substrate are shown in Fig. 12(c) and (d), where no significant substrate deformation, even after substrate preheating, was observed. The Ti6Al4V preheated substrate deformation depth was measured to be $0.8 \pm 1.3 \mu\text{m}$ and was very similar to the deformation depth of the non-preheated substrate at $0.5 \pm 1.3 \mu\text{m}$ at 834 m/s deposition condition. Ti6Al4V retains its specific strength up to 500 °C (Ref 39) and higher substrate pre-heat temperatures are needed to induce substrate deformation.

The flattening ratio for Ti and Ti6Al4V splats deposited on preheated substrates is shown in Fig. 13(a) and (b). The splat flattening ratio for Ti splats on preheated Ti substrate demonstrated a slight decrease when compared to the same splats deposited on unheated substrates. This behavior can be explained by the substrate deformation observed in Fig. 12(b). On the other hand, the flattening ratio of Ti6Al4V splats deposited on preheated substrates

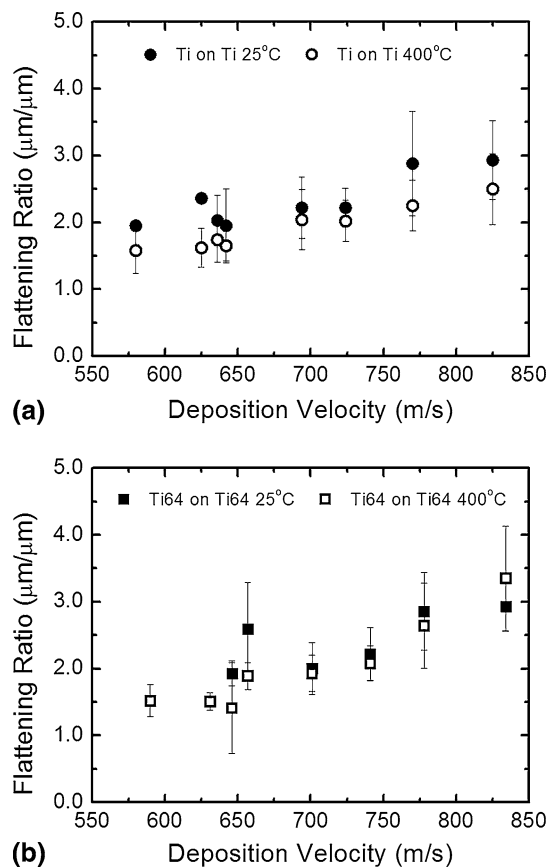


Fig. 13 Flattening ratio of (a) Ti splats deposited on Ti substrate at 25 °C and preheated to 400 °C and (b) Ti6Al4V splats deposited on Ti6Al4V substrate at 25 °C and preheated to 400 °C. The flattening ratio decreases for Ti splats deposited on preheated substrate. No change in the flattening ratio was measured for Ti64 splats deposited on Ti64 substrate at 25 °C or at 400 °C

was similar to that of Ti6Al4V splats on unheated substrates as shown in Fig. 13(c). The results correlate well with the SEM images shown in Fig. 12(c) and (d) where no substrate deformation was observed.

Unlike the similarity for flattening ratios from preheated and unheated substrates, a dramatic increase in the splat adhesion strength was measured for Ti and Ti6Al4V splats deposited on preheated substrates. In Fig. 14(a), the adhesion strength of Ti splats reached ~250 MPa at a deposition velocity of 700 m/s, a significant improvement from 100 to 120 MPa measured for the same velocity splats on unheated substrates. A similar increase in the adhesion strength was measured for Ti6Al4V splats deposited at slightly higher deposition velocity of 700 m/s in Fig. 14(b).

For Ti splats deposited on preheated substrates, the regime 3 behavior was observed for deposition velocities at or above 825 m/s. For non-preheated substrates, this occurred at a much higher velocity of 1140 m/s. For Ti6Al4V splats deposited on preheated substrates, splats deposited at or above 834 m/s exhibited regime 2 behavior, much lower than the 1115 m/s observed in splats deposited on the unheated substrates.

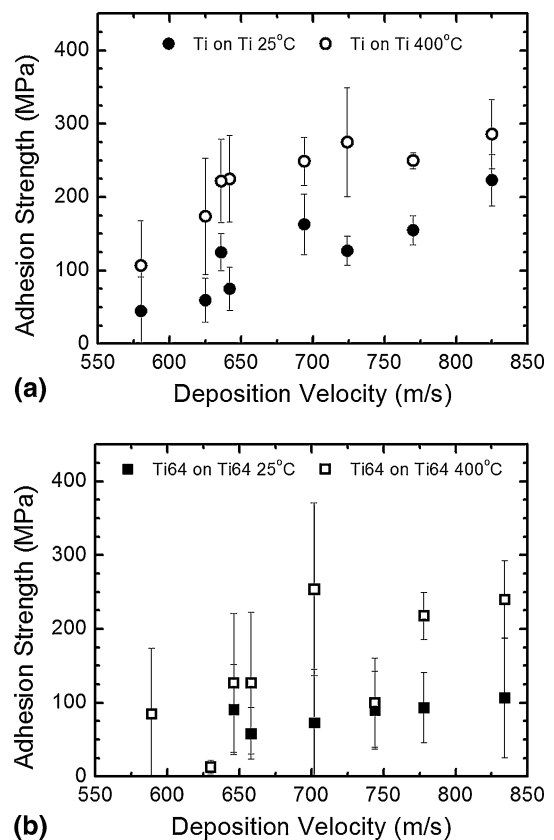
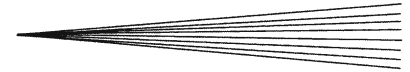


Fig. 14 Splat adhesion strength as a function of deposition velocity for (a) Ti splats deposited on Ti substrate at 25 °C and preheated to 400 °C and (b) Ti6Al4V splats deposited on Ti6Al4V substrate at 25 °C and preheated to 400 °C. The adhesion strength is higher for splats deposited on preheated substrate



4. Discussion

The most widely accepted mechanism for metallurgical bonding in cold sprayed metals is the formation of adiabatic shear instability (Ref 1, 3, 8, 40). The ability of a cold sprayed particle to undergo plastic deformation and adiabatic shear is a function of material properties, such as yield strength and melting point as well as process conditions, such as deposition temperature, particle velocity and particle size (Ref 3, 8, 10, 41). When a particle arrives at the substrate at its critical velocity, adiabatic shear takes place, which then contributes to a formation of a metallurgical bonding (Ref 5, 12). However, even when a coating is created with average in-flight particle velocity well above the critical velocity, incomplete bonding is often observed (Ref 6, 11, 16). This is especially true for materials with high melting point and high yield strength, like Ti and its alloys (Ref 3).

The cold spray process is somewhat complex and the effects of particle or substrate characteristics, temperature, gas flow and the nozzle design on the quality of cold spray deposits are not easy to evaluate using experimental methods. Many studies instead make use of computational simulations (Ref 2, 3, 5, 24). The technique used here measures bond strength at the splat level, which is the level where the basic mechanism of adiabatic shear instability takes place. Identification of the effect of processing parameters on the underlying mechanism of adiabatic shear instability and the extent to which bonding occurs at the splat level is one viable way to gather information useful to optimizing the cold spray process. The splat adhesion test (Ref 11) can directly address the effect of the process conditions on bonding of cold spray splats. Thus, process parameters for cold spray can be explored without spraying large quantities of material to identify the best conditions leading to sufficient adiabatic shear for a formation of a continuous and strong bonding.

One important processing consideration is the effect of non-uniform distribution of velocity across the gas jet. Many simulations have indicated that particle velocity is not continuous and varies depending on the particle position in the gas jet (Ref 24, 42, 43). Zahiri et al. demonstrated that the particles traveling at the center of the gas jet had a higher particle velocity when compared to the particles traveling at the edge of the gas jet (Ref 24, 43). As was seen in Fig. 11, the adhesion of splats deposited at the edges of the gas jet had lower adhesion (~20-100 MPa) compared to those arriving in near the center of the jet (~200 MPa). This effect was likely due to the drop-off in the velocity away from the center of the jet. The poor adhesion strength of particles at the edges of the gas jet can affect the mechanical integrity of the cold spray coatings. To optimize the deposition of hard to deposit materials, such as Ti and Ti6Al4V, a better design of the nozzle may be required (Ref 1, 42, 44). One work suggested, the use of a rectangular nozzle provided a more homogenous velocity distribution across the gas jet when compared to the circular nozzle (Ref 1). If in the future, high quality cold sprayed coatings of high melting point,

high strength materials (Ref 3) are to be realized, nozzle design and optimization of the gas flow will be significant contributions leading to success in this endeavor.

Feedstock particle size is another important processing parameter as different particle sizes lead to different velocities (Ref 2, 3, 37). Assuming one has already chosen an optimum range of particle sizes, within this size range, small particles travel at higher velocities than larger particles. At the same time the ability of smaller particle to undergo adiabatic shear is reduced and higher velocities are often required in order to deposit smaller particles when compared to particles of larger size (Ref 2, 3). The results from splat adhesion test showed that for Ti, the adhesion strength for smaller particles was higher when compared to larger particles. Particles with diameters of 15 μm or less had adhesion of roughly 300 MPa, while those with diameter surpassing 40 μm had adhesion on the order of 200 MPa. The ratio of the deposition velocity vs. critical velocity of smaller particles was, therefore, higher than for the larger particles. For these tests where we examined particle size, their size ranged from 10 to 60 μm and they were located at the center of the deposition pass. For these conditions, the effect of the particle size may not have played a substantial role on the adiabatic shear. Also the bow shock effect (Ref 1), where small particles deviate from the deposition trajectory, was not taken into account. Furthermore, the particles were deposited directly on the annealed substrate material. The effect of particle size on the particle bonding mechanisms in a coating subjected to high stress may be different (Ref 3, 28). Additional studies on the particle size effect on the deposition efficiency and structural integrity of Ti and Ti6Al4V cold spray coating may provide additional insight on the effect of particle size beyond what has been shown here.

The material composition had a significant effect on cold spray deposition. The adhesion strength of Ti splats deposited on Ti was consistently higher than the adhesion strength of Ti6Al4V splats deposited on Ti6Al4V substrate. This behavior can be explained by a significantly higher yield strength of Ti6Al4V at 1200 MPa when compared to that of pure Ti at 700 MPa (Ref 7). The yield strength of the material affects the critical velocity required to induce adiabatic shear and therefore the ability of the material to form a strong, metallurgical bond (Ref 3, 8).

For cold spray, increasing temperature has the beneficial effect reducing the yield strength of the sprayed material (Ref 45). The gas interaction with the feed-stock powder and substrate as well as the particle impact with the substrate will all increase the temperature both locally and globally (Ref 1, 2, 5, 38). According to Schmidt et al., using calculations done for copper particles, the particle temperature can reach up to 200 °C in the gas preheated to 600 °C (Ref 2). With increase in the temperature, the shear strength of Ti6Al4V subjected to high strain rates decreases (Ref 45) an effect that will lead to an earlier onset of adiabatic shear instability and better material bonding. For Ti6Al4V splats deposited on Ti6Al4V substrate at 650 and 850 m/s, the use of nitrogen gas,

preheated to higher temperatures than helium, resulted in a slight increase in the adhesion strength (~50 MPa) (see Fig. 7b). For Ti, where the shear stress is considerably lower than that of the alloy, the effect of the gas preheat temperature on particle adhesion was more subtle but still noticeable. For deposition velocity between 600 and 650 m/s, the adhesion strength of splats can be ranked with gas temperature. The highest adhesion strength was for splats deposited with nitrogen at 500 °C followed by those with nitrogen at 300 °C and lastly by those with helium at 50 °C. However, at higher deposition velocities, which clearly exceed the critical velocity for Ti, there was no difference due to gas temperature. For example, at a deposition velocity of roughly 800 m/s, the adhesion strength was nearly identical for splats deposited with nitrogen at 800 °C and those deposited with helium at 50 °C.

Particles sprayed with higher gas pre-heat temperatures are expected to retain some thermal energy and arrive at the substrate at a higher temperature than those with lower gas pre-heat temperatures. The gas pre-heat temperature via the gas jet can also affect the substrate; however, the deposition of the splats was carried out with a single pass at a high transverse velocity. Thus, the gas interaction with the substrate material was limited. In terms of cold spray coatings, it is important to note that the gas temperature will increase the substrate temperature given enough time (Ref 1). Legoux et al. (Ref 38), using an infrared camera, measured temperatures upwards of 330 °C in regions of a substrate subjected to a stationary impact with nitrogen gas preheated to 500 °C and passed through a cold spray nozzle. Such increase in the temperature can reduce the shear stress of Ti6Al4V and can affect the deformation and adhesion mechanisms of the material (Ref 45, 46). To evaluate the effect of the substrate temperature on the deposition of the cold spray splats, Ti and Ti6Al4V splats were deposited on Ti or Ti6Al4V substrates preheated to 400 °C. An increase of over 100 MPa in adhesion strength was measured in both cases. Furthermore, near ideal shearing behavior, regime 3 behavior, was observed for Ti splats deposited at 825 m/s on preheated Ti substrate as opposed to 1140 m/s in case of an unheated substrate. Ti6Al4V splats also demonstrated an improvement in the splat adhesion behavior. Ti6Al4V splats deposited at 834 m/s on preheated Ti6Al4V substrate sheared according to the regime 2, whereas same splats deposited on unheated substrate sheared according to regime 1. In regime 2 shearing behavior material demonstrates regions with a ductile fracture, shown in Fig. 9, which is indicative of a partial metallurgical bonding, whereas in regime 1, the particles adhered mainly through a weaker conformal adhesion.

The flattening ratio did not reflect the drastic increase in the splat adhesion strength seen in Ti splats deposited with helium gas in Fig. 7(a) and on preheated substrates in Fig. 13. Our results indicate that the splat flattening ratio, while a good indicator of the extent of plastic deformation, and to some extent adiabatic shear (e.g. jetting), is not necessarily a good indicator for bonding and splat adhesion strength. Thus, to fully explicate the splat bonding and the portion of the adiabatic shear process that leads to

bonding, other parameters must be considered, such as: strain rate, stress localization, temperature, and the conformity of the interface between the adiabatic shear instability region and the substrate material which is enhanced through substrate deformation.

Splat adhesion testing can be used to measure the adhesion strength and identify bonding mechanisms for the individual cold spray splats based on the appearance of the load-displacement curves (i.e. the regime assignments made here). The height, the width, and the shape of the load-displacement curves were used to define the strength, the type, and the continuity of the bonded interface between splat and substrate material at any location in the deposition pass. Guetta et al. (Ref 9) also measured the adhesion strength of splats with a LASAT. LASAT measures the tensile stress required to de-bond splats over a 1 cm region in the substrate and is, therefore, less sensitive to the adhesion strength of individual splats and their position in the substrate. LASAT was, however, used to measure the adhesion strength of splats imbedded in the substrate and the adhesion strength of cold spray coatings (Ref 9, 47).

Most adhesion testing techniques are designed for the bond strength of coating to substrate, similar to the standard, ASTM C-633-99. All of these suffer from issues with epoxy strength that limits that maximum strength that may be measured. For example, in a hydraulic adhesion/tensile test, the coating is typically glued to two circular elements with a heat cured epoxy and then pulled apart (Ref 5, 48). The hydraulic adhesion/tensile test was used by Price et al. (Ref 48) to measure the bond strength of Ti coating deposited on as-received and grit blasted Ti6Al4V substrate. The coatings were deposited at 500 m/s and the bond strength was measured to be 32-37 MPa (Ref 48). Using similar methods, Morrocco et al. (Ref 49) measured the bond strength Ti coatings on polished, grit blasted or ground Ti6Al4V substrates. The bond strength was found to be between 5 and 25 MPa. Bae et al. (Ref 5), measured the bond strength of Ti coatings deposited at 650 m/s on steel substrates. The bond strength was measured to be between 49 and 69 MPa. In most cases, the failure occurred in the epoxy, failing at 85 MPa, and the bond strength of the coatings deposited at higher deposition velocities could only be reported as greater than 85 MPa (Ref 5, 48).

The cohesive strength between particles within coatings is also of particular interest and can be measured by a recently developed technique called the tubular coating tensile (TCT) test. The method was first developed by Schmidt et al. for the measurement of the cohesive strength of copper cold spray particles in the coating deposited on the aluminum substrate (Ref 2). More recently, Binder et al. used TCT test to measure the cohesive strength of cold sprayed Ti particles in coatings deposited with nitrogen gas at pre-heat temperatures from 600 to 1000 °C (Ref 21). The coatings were deposited with a Kinetiks 8000 Cold Spray Gun and spherical Ti powder with 33.5 μm average diameter. The deposition velocities were not measured but were calculated to range between 650 and 800 m/s for 25 μm particles (Ref 21).

Interesting correlations were found between the cohesive strength in Ti coating sprayed by Binder et al. (Ref 21) and the adhesion strength of Ti splats sprayed for this study (see Fig. 15). In general, particle cohesion strength for Ti correlated well with the adhesion strength of Ti splats. For deposition velocities below 700 m/s, the magnitude of the cohesive strength matches the splat adhesion strength on unheated substrates very well and a similar trend with velocity was seen in both datasets. However, at higher velocities (>700 m/s) that are only achievable with high gas pre-heat temperatures, the cohesive strength was higher than the splat adhesion strength. This is likely an effect of the gas jet heating the substrate and coating during deposition, leading to an enhancement to the metallurgical bonding. This hypothesis is further supported by a comparison between the cohesive strength and the data for splat adhesion strength on heated substrates. At velocities below 700 m/s, the splat adhesion strength on heated substrates is higher than the cohesive strength. At these velocities, the gas preheat temperature used for a coating is lower and temperature effects are reduced. Thus, a splat on pre-heated substrate at these velocities should have a stronger bond. For higher deposition velocities (>700 m/s), where gas jet heating is more significant, the cohesive strength and splat adhesion strength on heated substrates agree very well. In a previous study, we observed a similar correlation between cohesive strength and splat adhesion strength (Ref 25), but the comparison made here between Binder et al. (Ref 21) and our measurements of splat adhesion strength is the first time that both the effect of velocity and temperature have been correlated in this way for the coating and splat levels.

Our splat adhesion test was shown to reveal trends for adhesion strength versus deposition velocity or temperature that are relevant to the bonding for a full coating, both between coating and substrate and cohesive strength within the coating. Also, the small scale precision of the method was useful for tracking the effects of particle size and position in the gas jet on the adhesion strength of splats. These are two variables that are known to have an effect, but are nearly impossible to measure experimentally

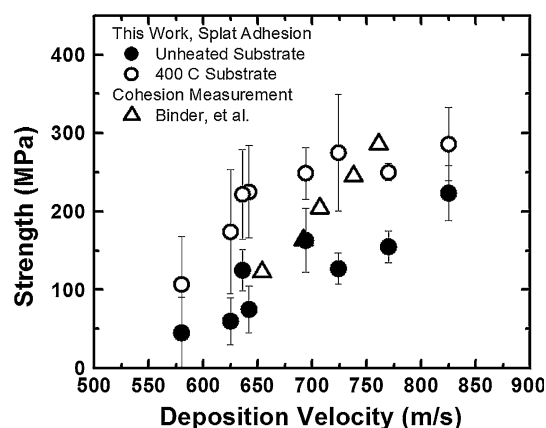


Fig. 15 A plot of splat adhesion strength (measured here) and cohesive strength (Ref 21) vs. deposition velocity. All data presented is for Ti sprayed with nitrogen as the propelling gas

with conventional techniques. There are, however, a few limitations for the current technique that merit mentioning. First, the adhesion testing cannot be carried on the splats deposited on top of very rough substrates. The roughness of the substrate will contribute to the noise in the measurements and if the roughness is high enough it would completely prevent a splat from being tested. Also, splats that are embedded in the substrate cannot be tested. Splats tested here, had at most 40% of their height below the substrate and were easily tested. However, as the extent of embedding increases, not only will the error on the measurement increase but the splat will eventually become untestable. Despite these small drawbacks to the technique, it is applicable to most materials being cold sprayed and provides valuable information on the connection between adhesion strength and process conditions at the splat level, which does not require a significant investment in quantity of sprayed material. However, we note that, like any micromechanical test, a better understanding of the splat adhesion test would be gained by a thorough finite element analysis (FEA). For example, the ball-bond shear test for solder joints was recently reviewed and examined with FEA to explore small variations in test conditions and their effect on the experimental results (Ref 50). For the splat adhesion test, questions about splat embedding, splat shape, defects at the splat/substrate interface and their relationship with fracture modes and failure mechanisms should be addressed in a similar manner.

5. Conclusion

A splat adhesion technique, also called the modified ball-bond shear test, was used to examine the effect of the deposition velocity, gas temperature, substrate temperature and particle size on the adhesion strength of Ti and Ti6Al4V splats deposited on Ti or Ti6Al4V substrates. Strong adhesion strength approaching the bulk shear strength was measured for Ti splats deposited on Ti substrates at velocities significantly higher (e.g. 1140 m/s) than the critical velocity. Ti6Al4V splats deposited on Ti6Al4V substrate demonstrated poor particle adhesion and a bonded interface that was not fully continuous, with only traces of metallurgical bonding, even at deposition velocities of 1115 m/s.

An increase in the adhesion strength of splats was measured with preheating of the Ti and Ti6Al4V substrates to 400 °C. A nearly ideal shearing behavior with fully bonded splat/substrate interface and adhesion strength of 284 MPa was observed for Ti deposited at 825 m/s on preheated substrates. Preheating of Ti6Al4V substrates also had a significant effect on the splat adhesion strength for Ti6Al4V splats, raising the splat adhesion strength from 100 to 250 MPa. A combination of high velocities, preheating of the powder and substrate may be a key to the deposition of Ti6Al4V with adhesion strength that approaches the strength found in Ti6Al4V made by traditional methods.

The adhesion strength of splats was found to vary with particle size and particle position in the deposition pass. Particle deposited at the center of the deposition pass and of smaller particle diameter showed superior adhesion strength when compared to the large particles or particles at the edge of the deposition pass.

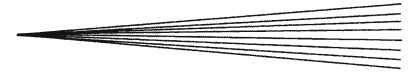
The extent of particle deformation measured in terms of splat flattening ratio, did not reflect well the degree of splat adhesion. The deformation of the substrate, on the other hand, was found to have a beneficial effect on the particle adhesion attributed to a confinement of the adiabatic shear region within the splat/substrate interface leading to a more successful metallurgical bonding.

Acknowledgments

The cold spray equipment was provided by CFI Project No. 8246, McGill University. The authors acknowledge the technical assistance of Bernard Harvey, Mario Lamontagne, Jean-Francois Alarie and Frederic Belval. The authors would also like to thank Jolanta Klemberg-Sapieha at Ecole Polytechnique for access to the instrument used for splat adhesion testing.

References

1. A. Papyrin, V. Kosarev, K.V. Klinkov, A. Alkimov, and V.M. Fomin, *Cold Spray Technology*, Chs. 1-3, Elsevier, 2007
2. T. Schmidt, F. Gaertner, and H. Kreye, New Developments in Cold Spray Based on Higher Gas and Particle Temperatures, *J. Therm. Spray Technol.*, 2006, **15**(4), p 488-494
3. T. Schmidt, F. Gärtner, H. Assadi, and H. Kreye, Development of a Generalized Parameter Window for Cold Spray Deposition, *Acta Mater.*, 2006, **54**(3), p 729-742
4. M. Grujicic, C.L. Zhao, W.S. DeRosset, and D. Helfritsch, Adiabatic Shear Instability Based Mechanism for Particles/Substrate Bonding in the Cold-Gas Dynamic-Spray Process, *Mater. Des.*, 2004, **25**(8), p 681-688
5. G. Bae, S. Kumar, S. Yoon, K. Kang, H. Na, H.J. Kim, and C. Lee, Bonding Features and Associated Mechanisms in Kinetic Sprayed Titanium Coatings, *Acta Mater.*, 2009, **57**(19), p 5654-5666
6. G. Bae, Y. Xiong, S. Kumar, K. Kang, and C. Lee, General Aspects of Interface Bonding in Kinetic Sprayed Coatings, *Acta Mater.*, 2008, **56**(17), p 4858-4868
7. J. Vlcek, L. Gimeno, H. Huber, and E. Lugscheider, A Systematic Approach to Material Eligibility for the Cold-Spray Process, *J. Therm. Spray Technol.*, 2005, **14**(1), p 125-133
8. H. Assadi, F. Gärtner, T. Stoltenhoff, and H. Kreye, Bonding Mechanism in Cold Gas Spraying, *Acta Mater.*, 2003, **51**(15), p 4379-4394
9. S. Guetta, M. Berger, F. Borit, V. Guipont, M. Jeandin, M. Boustie, Y. Ichikawa, K. Sakaguchi, and K. Ogawa, Influence of Particle Velocity on Adhesion of Cold-Sprayed Splats, *J. Therm. Spray Technol.*, 2009, **18**(3), p 331-342
10. D. Goldbaum, R.R. Chromik, S. Yue, E. Irissou, and J.-G. Legoux, Mechanical Property Mapping of Cold Spray Ti Splats, *J. Therm. Spray Technol.*, 2011, **20**(3), p 486-496
11. R.R. Chromik, D. Goldbaum, J.M. Shockley, S. Yue, E. Irissou, J.-G. Legoux, and N.X. Randall, Modified Ball Bond Shear Test for Determination of Adhesion Strength of Cold Spray Splats, *Surf. Coat. Technol.*, 2010, **205**(5), p 1409-1414
12. J. Vlcek, H. Huber, H. Voggenreiter, and E. Lugscheider, "Melting Upon Particle Impact in the Cold Spray Process," presented at Materials Week 2002, International Congress on Advanced Materials, Their Processes and Applications (Munich, Germany), Deutsche Gesellschaft für Materialkunde (DGM), Sept 2002
13. S. Guetta, M.H. Berger, F. Borit, V. Guipont, M. Jeandin, F. Evry, M. Boustie, F. Poitiers, Y. Ichikawa, K. Ogawa, and J. Sendai, Influence of Particle Velocity on Adhesion of Cold-Sprayed Splats, *Thermal Spray Conference & Exposition: Thermal Spray Crossing Borders*, ASM International, 2008, p 726-731
14. S. Yoon, H.J. Kim, and C. Lee, Deposition Behaviour of Bulk Amorphous NiTiZrSiSn According to the Kinetic and Thermal Energy Levels in the Kinetic Spraying Process, *Surf. Coat. Technol.*, 2006, **200**(20-21), p 6022-6029
15. X. Zhou, X. Wu, J. Wang, and J. Zhang, Numerical Investigation of the Rebounding and The Deposition Behavior of Particles During Cold Spraying, *Acta Metall. Sin. (English Lett.)*, 2011, **24**(1), p 45-53
16. K. Kim, M. Watanabe, K. Mitsuishi, K. Iakoubovskii, and S. Kuroda, Impact Bonding and Rebounding Between Kinetically Sprayed Titanium Particle and Steel Substrate Revealed by High-Resolution Electron Microscopy, *J. Phys. D Appl. Phys.*, 2009, **42**(6), p 65304-65308
17. K. Kim, M. Watanabe, J. Kawakita, and S. Kuroda, Effects of Temperature of In-Flight Particles on Bonding and Microstructure in Warm-Sprayed Titanium Deposits, *J. Therm. Spray Technol.*, 2009, **18**(3), p 392-400
18. C. Borchers, F. Gärtner, T. Stoltenhoff, and H. Kreye, Microstructural Bonding Features of Cold Sprayed Face Centered Cubic Metals, *J. Appl. Phys.*, 2004, **96**(8), p 4288-4292
19. T. Hussain, D. McCartney, P. Shipway, and D. Zhang, Bonding Mechanisms in Cold Spraying: The Contributions of Metallurgical and Mechanical Components, *J. Therm. Spray Technol.*, 2009, **18**(3), p 364-379
20. W. Wong, E. Irissou, A. Ryabinin, J.-G. Legoux, and S. Yue, Influence of Helium and Nitrogen Gases on the Properties of Cold Gas Dynamic Sprayed Pure Titanium Coatings, *J. Therm. Spray Technol.*, 2011, **20**(1), p 213-226
21. K. Binder, J. Gottschalk, M. Kollenda, F. Gärtner, and T. Klassen, Influence of Impact Angle and Gas Temperature on Mechanical Properties of Titanium Cold Spray Deposits, *J. Therm. Spray Technol.*, 2011, **20**(1-2), p 234-242
22. E. Irissou, J.G. Legoux, C. Moreau, and A.N. Ryabinin, How Cold is Cold Spray? An Experimental Study of the Heat Transfer to the Substrate in Cold Gas Dynamic Spraying, *International Thermal Spray Conference & Exposition: Thermal Spray Crossing Borders*, Jun 2-4, 2008 (Maastricht, Netherlands), 2008
23. P.C. King and M. Jahedi, Relationship Between Particle Size and Deformation in the Cold Spray Process, *Appl. Surf. Sci.*, 2010, **256**(6), p 1735-1738
24. S. Zahiri, W. Yang, and M. Jahedi, Characterization of Cold Spray Titanium Supersonic Jet, *J. Therm. Spray Technol.*, 2009, **18**(1), p 110-117
25. D. Goldbaum, J. Ajaja, R.R. Chromik, W. Wong, S. Yue, E. Irissou, and J.-G. Legoux, Mechanical Behavior of Ti Cold Spray Coatings Determined by a Multi-Scale Indentation Method, *Mater. Sci. Eng. A*, 2011, **530**, p 253-265
26. G. Clatterbaugh, J. Weiner, and H. Charles, Jr., Gold-Aluminum Intermetallics: Ball Bond Shear Testing and Thin Film Reaction Couples, *IEEE Trans. Compon. Hybrids Manuf. Technol.*, 1984, **7**(4), p 349-356
27. M.E. Dickinson and M. Yamada, A New Method for Measuring Shear Adhesion Strength of Ceramic Cold Spray Splats, *Nanosci. Nanotechnol. Lett.*, 2010, **2**, p 348-351
28. W. Wong, A. Rezaeian, E. Irissou, J.G. Legoux, and S. Yue, Cold Spray Characteristics of Commercially Pure Ti and Ti-6Al-4V, *Adv. Mater. Res.*, 2010, **89-91**, p 639-644
29. G.F. Vander Voort, *Metallography, Principles and Practice*, ASM International, Materials Park, OH, 1999
30. R. Kapoor and S. Nemat-Nasser, Determination of Temperature Rise During High Strain Rate Deformation, *Mech. Mater.*, 1998, **27**(1), p 1-12



31. W.C. Oliver and G.M. Pharr, An Improved Technique for Determining Hardness and Elastic Modulus Using Load and Displacement Sensing Indentation Experiments, *J. Mater. Res.*, 1992, **7**(6), p 1564-1583
32. R. Boyer, G. Welsch, and E.W. Collings, Ed., *Materials Property Handbook: Titanium Alloys*, ASM International, 1994
33. W.-Y. Li, C. Zhang, X. Guo, J. Xu, C.J. Li, H. Liao, C. Coddet, and K.A. Khor, Ti and Ti-6Al-4V Coatings by Cold Spraying and Microstructure Modification by Heat Treatment, *Adv. Eng. Mater.*, 2007, **9**(5), p 418-423
34. W.-Y. Li, C. Zhang, X. Guo, C.-J. Li, H. Liao, and C. Coddet, Study on Impact Fusion at Particle Interfaces and Its Effect on Coating Microstructure in Cold Spraying, *Appl. Surf. Sci.*, 2007, **254**(2), p 517-526
35. G. Lutjering and J.C. Williams, *Titanium*, Springer, New York, 2003, p 190
36. V.A. Joshi, *Titanium Alloys: An Atlas of Structures and Fracture Features*, CRC Taylor & Francis Group, Boca Raton, 2006, p 1-2
37. B. Samareh and A. Dolatabadi, A Three-Dimensional Analysis of the Cold Spray Process: The Effects of Substrate Location and Shape, *J. Therm. Spray Technol.*, 2007, **16**(5), p 634-642
38. J. Legoux, E. Irissou, and C. Moreau, Effect of Substrate Temperature on the Formation Mechanism of Cold-Sprayed Aluminum, Zinc and Tin Coatings, *J. Therm. Spray Technol.*, 2007, **16**(5), p 619-626
39. C. Leyens and M. Peters, Ed., *Titanium and Titanium Alloys: Fundamentals and Applications*, Wiley-VCH Verlag GmbH & Co., 2003, p 3
40. M. Grujicic, Particle/Substrate Interaction in the Cold-Spray Bonding Process, Ch. 9, *The Cold Spray Materials Deposition Process: Fundamentals and Applications*, V.K. Champagne, Ed., Woodhead Publishing Limited, 2007
41. C.-J. Li, W.-Y. Li, and H. Liao, Examination of the Critical Velocity for Deposition of Particles in Cold Spraying, *J. Therm. Spray Technol.*, 2006, **15**(2), p 212-222
42. A. Alkhimov, V. Kosarev, and S. Klinkov, The Features of Cold Spray Nozzle Design, *J. Therm. Spray Technol.*, 2001, **10**(2), p 375-381
43. V. Kosarev, S. Klinkov, A. Alkhimov, and A. Papyrin, On Some Aspects of Gas Dynamics of the Cold Spray Process, *J. Therm. Spray Technol.*, 2003, **12**(2), p 265-281
44. B. Samareh, O. Stier, V. Lüthen, and A. Dolatabadi, Assessment of CFD Modeling via Flow Visualization in Cold Spray Process, *J. Therm. Spray Technol.*, 2009, **18**(5), p 934-943
45. P. Follansbee and G. Gray, An Analysis of the Low Temperature, Low and High Strain-Rate Deformation of Ti-6Al-4V, *Metall. Mater. Trans. A*, 1989, **20**(5), p 863-874
46. M. Vanderhastan, L. Rabet, and B. Verlinden, AME High Temperature Deformation of Ti6Al4V at Low Strain Rate, *Metallurgija*, 2005, **11**, p 195-200
47. V. Guipont, M. Jeandin, S. Bansard, K.A. Khor, M. Nivard, L. Berthe, J.-P. Cuq-Lelandais, and M. Boustie, Bond Strength Determination of Hydroxyapatite Coatings on Ti-6Al-4V Substrates Using the LASER Shock Adhesion Test (LASAT), *J. Biomed. Mater. Res. A*, 2010, **95A**(4), p 1096-1104
48. T. Price, P. Shipway, and D. McCartney, Effect of Cold Spray Deposition of a Titanium Coating on Fatigue Behavior of a Titanium Alloy, *J. Therm. Spray Technol.*, 2006, **15**(4), p 507-512
49. T. Marrocco, D. McCartney, P. Shipway, and A. Sturgeon, Production of Titanium Deposits by Cold-Gas Dynamic Spray: Numerical Modeling and Experimental Characterization, *J. Therm. Spray Technol.*, 2006, **15**(2), p 263-272
50. J.-W. Kim and S.-B. Jung, Reexamination of the Solder Ball Shear Test for Evaluation of the Mechanical Joint Strength, *Int. J. Solids Struct.*, 2006, **43**(7-8), p 1928-1945